Inorganic Chemistry

including bioinorganic chemistry

January 6, 2014
Volume 53, Number 1
pubs.acs.org/IC

Observing the Activation of Water Oxidation Catalysts

ACS Publications
MOST TRUSTED. MOST CITED. MOST READ.

www.acs.org

Inorganic Chemistry

JANUARY 6, 2014
VOLUME 53 ISSUE 1
INOCAJ 53(1) 1−660 (2014)
ISSN 0020-1669
Registered in the U.S. Patent and Trademark Office

ON THE COVER: Complex speciation during the activation of organometallic iridium water/C−H oxidation precatalysts is revealed by in operando electrospray mass spectrometry. See A. J. Ingram, A. B. Wolk, C. Flender, J. Zhang, C. J. Johnson, U. Hintermair, R. H. Crabtree, M. A. Johnson, and R. N. Zare, p 423. Cover design by Catharine L. Wallace.

Editorial

Communications

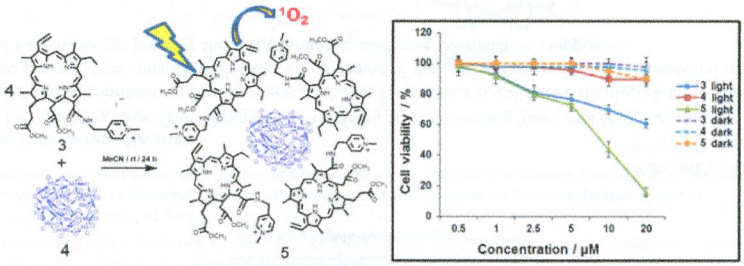

6 Ⓢ dx.doi.org/10.1021/ic402160h

A Cyanide-Bridged Molybdenum Bis(maleonitriledithiolate) Square

Moumita Bose, Golam Moula, and Sabyasachi Sarkar*

The rare cyano-bridged molybdenum square capped with radical dithiolenes displays strong inter- and intramolecular antiferromagnetic interactions.

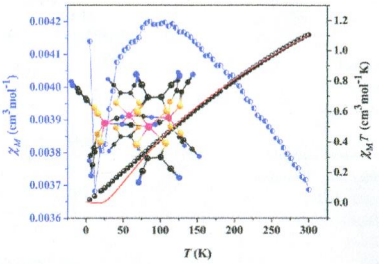

9 Ⓢ dx.doi.org/10.1021/ic4021993

Effect of Local Structure Distortion on Superconductivity in Mg- and F-Codoped $LaOBiS_2$

Haijie Chen, Ganghua Zhang, Tao Hu, Gang Mu, Wei Li, Fuqiang Huang,* Xiaoming Xie, and Mianheng Jiang

The crystal structure of $LaOBiS_2$ is composed of two alternative layered motifs with charge-positive and -negative layers, similar to the well-known Fe-based LaOFeAs. Mg^{2+} and F^- were codoped into the lattice of $LaOBiS_2$ to explore the effect of local structure distortion on superconductivity.

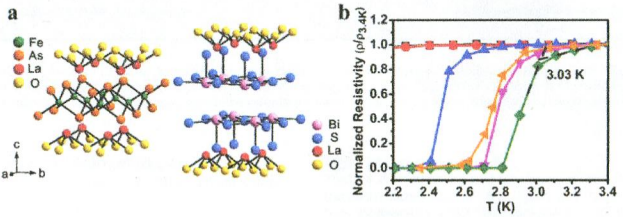

12 Ⓢ dx.doi.org/10.1021/ic402315a

Room Temperature Rapid Functionalization of E–H Bonds (E = O, N, S) via the Metal–Ligand Cooperation Mechanism

Adam Scharf, Israel Goldberg, and Arkadi Vigalok*

A PNF-type palladium complex strips water and anilines of both hydrogen atoms rapidly and efficiently. The reaction with thiols depends on the nature of the substituent at the sulfur atom, with thiophenols giving products of C–S elimination.

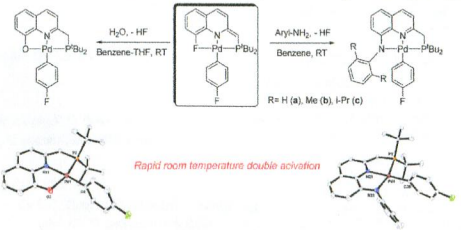

15 S dx.doi.org/10.1021/ic402407k

Synthesis and Characterization of a High-Symmetry Ferrous Polypyridyl Complex: Approaching the $^5T_2/^3T_1$ Crossing Point for Fe^{II}

Lindsey L. Jamula, Allison M. Brown, Dong Guo, and James K. McCusker*

The synthesis, physical, and photophysical properties of the first member of a new class of iron(II) polypyridyl complexes are described. The near-perfect O_h symmetry and strong ligand field, coupled with an unusually short excited-state lifetime, suggest that this compound sits at or near the $^5T_2/^3T_1$ term-state crossing point expected for a d^6 transition-metal complex.

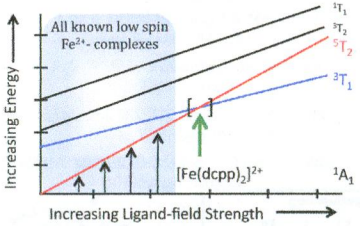

18 S dx.doi.org/10.1021/ic4024184

Open Pentameric Calixarene Nanocage

Kongzhao Su, Feilong Jiang, Jinjie Qian, Mingyan Wu, Yanli Gai, Jie Pan, Daqiang Yuan, and Maochun Hong*

A novel open helmetlike coordination cage has been synthesized based on Co_4-calixarene shuttlecock-like secondary building units and in situ generated phosphate ligands, where the opening of the cage comprises a large 16-membered ring. The above unprecedented Co_{20} nanocage presents the first pentameric calixarene coordination compound.

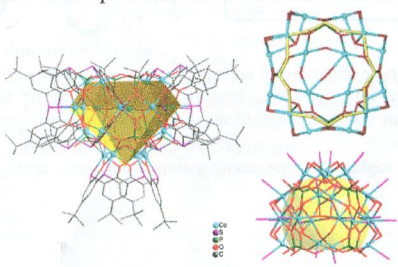

21 S dx.doi.org/10.1021/ic4025684

Tetrachloridometallate Dianion-Induced Cucurbit[8]uril Supramolecular Assemblies with Large Channels and Their Potential Applications for Extraction Coating on Solid-Phase Microextraction Fibers

Ning-Ning Ji, Xiao-Jie Cheng, Yi Zhao, Li-Li Liang, Xin-Long Ni, Xin Xiao, Qian-Jiang Zhu, Sai-Feng Xue, Nan Dong,* and Zhu Tao*

In the present work, we present some porous supramolecular assemblies with the largest Q[8]-based channels in the presence of $[M_{d\text{-}block}Cl_4]^{2-}$ anions through ion−dipole interaction and hydrogen bonding between the dianion and ≡CH or =CH_2 groups on the backs of Q[8] molecules.

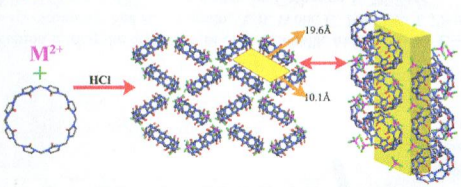

24 dx.doi.org/10.1021/ic402610q

Construction of an $M_3L_2A_6$ Cage with Small Windows from a Flexible Tripodal Ligand and Cu(hfac)$_3$

Mari Ikeda, Keiji Ohno, Yuki Kasumi, Shunsuke Kuwahara, and Yoichi Habata*

The construction of an $M_3L_2A_6$ cage with small windows from **L** and Cu(hfac)$_2$ is reported. Cold spray ionization mass spectrometry of a mixture of **L** and Cu(hfac)$_2$ indicated the formation of a $Cu_3L_2hfac_6$ cage in solution. X-ray crystallography showed that the $Cu_3L_2hfac_6$ cage contained neutral molecules such as THF and $CHCl_3$. The six hfac anions were critical to the neutral guest molecules being tightly held.

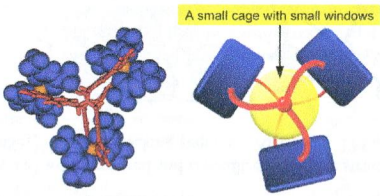

27 dx.doi.org/10.1021/ic402769u

Synthesis, Bonding, and Reactivity of a Cerium(IV) Fluoride Complex

Ursula J. Williams, Jerome R. Robinson, Andrew J. Lewis, Patrick J. Carroll, Patrick J. Walsh, and Eric J. Schelter*

Oxidation of Ce[N(SiMe$_3$)$_2$]$_3$ in the presence of PF_6^- or BF_4^- afforded isolation of CeF[N(SiMe$_3$)$_2$]$_3$. Structural, electrochemical, and spectroscopic characterization and density functional theory have been used to characterize this compound.

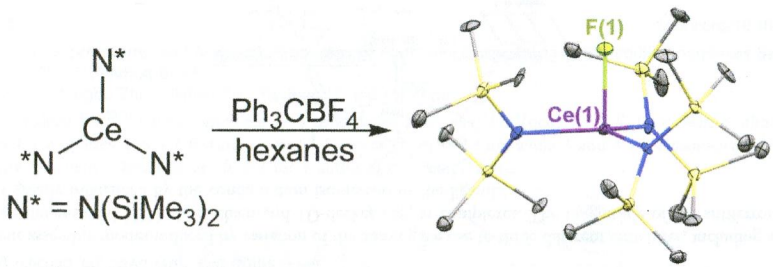

30 dx.doi.org/10.1021/ic402772j

Synthesis and Properties of the First [Au(dien)(N-heterocycle)]$^{3+}$ Compounds

Sarah R. Spell and Nicholas P. Farrell*

The solution properties of [Au(dien)(9-EtG)](NO$_3$)$_3$ show three pH-dependent species over a broad pH range. The use of N-heterocycle ligands modulates the reduction potential of gold(III) and the acidity of the dien moiety. The gold(III) compounds show significant enhancement of $\pi-\pi$-stacking interactions relative to their isostructural and isoelectronic platinum(II) and palladium(II) compounds

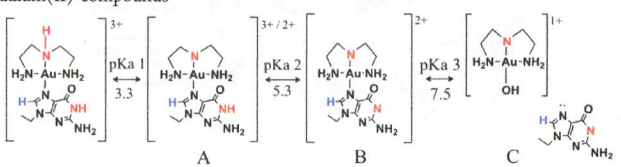

33 dx.doi.org/10.1021/ic402954p

1-Phenyl-3-(pyrid-2-yl)benzo[*e*][1,2,4]triazinyl: The First "Blatter Radical" for Coordination Chemistry

Ian S. Morgan,* Anssi Peuronen, Mikko M. Hänninen, Robert W. Reed, Rodolphe Clérac, and Heikki M. Tuononen

A neutral air- and moisture-stable N,N′-chelating radical ligand, 1-phenyl-3-(pyrid-2-yl)benzo[*e*][1,2,4]triazinyl (**1**) was synthesized and characterized by electron paramagnetic resonance spectroscopy, X-ray crystallography, magnetic measurements, and theoretical calculations. The coordination properties of **1** were verified by synthesis of the copper(II) complex Cu(**1**)(hfac)$_2$ in which the radical binds to the metal in a bidentate fashion. Radical **1** is a new addition to the growing library of 1,2,4-triazinyl radicals and the first member of this family synthesized specifically for coordination purposes.

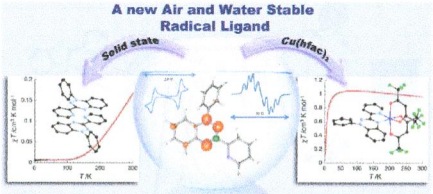

Articles

36 dx.doi.org/10.1021/ic401985d

Neutral, Cationic, and Anionic Low-Spin Iron(III) Complexes Stabilized by Amidophenolate and Iminobenzosemiquinonate Radical in *N,N,O* Ligands

Amit Rajput, Anuj K. Sharma, Suman K. Barman, Debasis Koley, Markus Steinert, and Rabindranath Mukherjee*

Using a new redox-active azo-appended tridentate ligand, H_2L = 2-(2- phenylazo)anilino-4,6-di-*tert*-butylphenol, complexes $[Fe^{III}(L)_2]$ (**1**) (X-ray), $[Fe^{III}\{(L^{ISQ})^{-\bullet}\}_2][BF_4]$ (**2**) (X-ray), and $[Co^{III}(\eta^5\text{-}C_{10}H_{15})_2][Fe^{III}\text{-}\{(L^{AP})^{2-}\}_2]$ (**3**) are synthesized. Detailed spectroscopic, redox, and DFT investigations have been performed to assign the oxidation and spin-state of iron and the oxidation level of the coordinated ligands in **1**−**3**. Existence of valence-tautomerism in **2** and **3** has been noted.

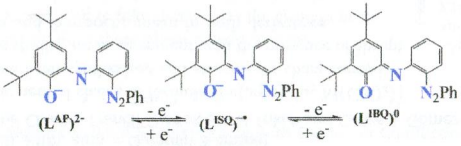

49 dx.doi.org/10.1021/ic401091r

Synthesis, Structure, and Properties of a Series of Chiral Tweezer−Diamine Complexes Consisting of an Achiral Zinc(II) Bisporphyrin Host and Chiral Diamine Guest: Induction and Rationalization of Supramolecular Chirality

Sanfaori Brahma, Sk Asif Ikbal, and Sankar Prasad Rath*

A series of supramolecular chiral tweezers consisting of an achiral Zn(II) bisporphyrin host and variety of chiral diamine guests have been presented here that demonstrate a full and unambiguous rationalization of the chirality transfer process from the chiral guest to the achiral host observed in many natural and artificial supramolecular assemblies.

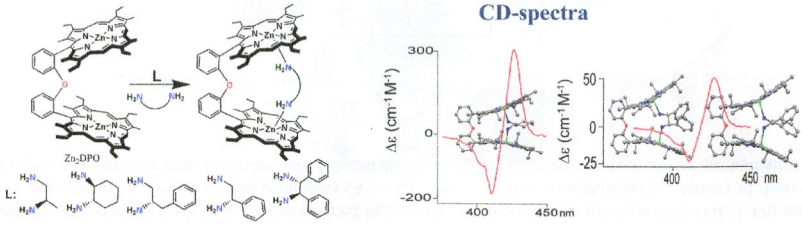

63 S dx.doi.org/10.1021/ic4012422

Polynuclear Complex Family of Cobalt(II)/Sulfonylcalixarene: One-Pot Synthesis of Cluster Salt $[Co_{14}^{II}]^{+}[Co_{4}^{II}]^{-}$ and Field-Induced Slow Magnetic Relaxation in a Six-Coordinate Dinuclear Cobalt(II)/Sulfonylcalixarene Complex

Meriem Lamouchi, Erwann Jeanneau, Ghenadie Novitchi, Dominique Luneau, Arnaud Brioude, and Cédric Desroches*

Starting from the same initial sulfonylcalixarene and cobalt salt mixture but varying the reaction time results in the formation of several new clusters, an original structure based on $[Co_{14}][Co_4]$ clusters was obtained, representing the first one-pot synthesis of a cobalt aggregate salt reported in the literature. The synthesis and magnetic properties of these cobalt compounds are discussed.

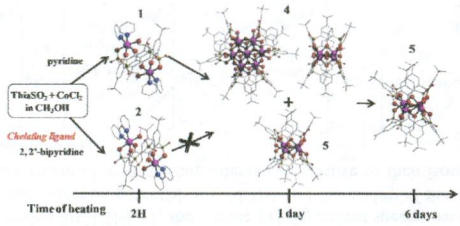

73 S dx.doi.org/10.1021/ic4014027

Anion-Tunable Configuration Isomerism and Magnetic Coupling in a Tetranuclear Discrete, One-Dimensional (1D) Chiral Chain and 1D-Decker Copper(II) Complexes of a Carbohydrazine Derivative

Wei Huang, Yuchao Jin, Dayu Wu,* and Genhua Wu

The different assembly modes induced by variation of the anion gave rise to three different structures, including a tetranuclear discrete, one-dimensional (1D) chiral chain and 1D-decker copper complexes. The magnitude of the antiferromagnetic coupling is greatly influenced by the configuration isomerism of the ligand.

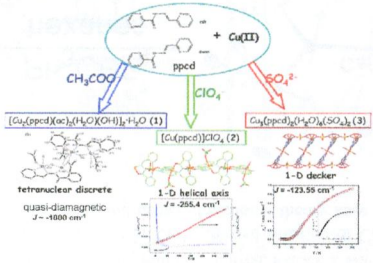

80 S dx.doi.org/10.1021/ic4013763

$Ba_3TM_2Se_9$ (TM = Nb, Ta): Synthesis and Characterization of New Polyselenides

Ming-Yan Chung and Chi-Shen Lee*

Polyselenides $Ba_3TM_2Se_9$ (TM = Nb, Ta) were prepared and crystallized in a new structural type. The 3D structures comprise distorted close-packed layers of $^{3}_{\infty}[BaSe_3]^{3.33-}$ with stacking sequence ABCACB. TM atoms occupy octahedral holes to form isolated $[(TM^{5+})_2(Se^{2-})_7(Se_2^{2-})]$ units.

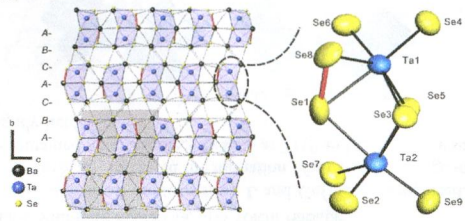

85 Ⓢ dx.doi.org/10.1021/ic4015493

Influence of the Coordination Environment of Zinc(II) Complexes of Designed Mannich Ligands on Phosphatase Activity: A Combined Experimental and Theoretical Study

Ria Sanyal, Averi Guha, Totan Ghosh, Tapan Kumar Mondal, Ennio Zangrando,* and Debasis Das*

Tuning of Mannich reaction leads to an unprecedented ligand (HL^1) along with the usual product (HL^2). On reaction with $Zn^{II}X_2$ they generate di- and mononuclear complexes ($X^- = Cl^-, Br^-, I^-$). The monophosphatase activity of those complexes has been explored where the role of halides, which is parallel to their electronegativity, is markedly prominent.

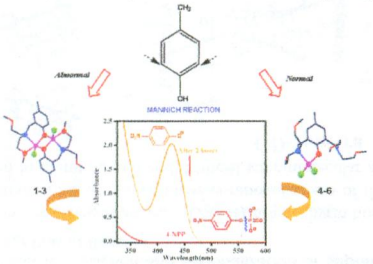

97 Ⓢ dx.doi.org/10.1021/ic401721x

Spin Crossover Iron(II) Coordination Polymer Chains: Syntheses, Structures, and Magnetic Characterizations of $[Fe(aqin)_2(\mu_2\text{-}M(CN)_4)]$ (M = Ni(II), Pt(II), aqin = Quinolin-8-amine)

Fatima Setifi, Eric Milin, Catherine Charles, Franck Thétiot, Smail Triki,* and Carlos J. Gómez-García

New Fe^{II} coordination polymeric neutral chains of formula $[Fe(aqin)_2(\mu_2\text{-}M(CN)_4)]$ (M = Ni^{II} (1) and Pt^{II} (2)) have been synthesized and structurally characterized. Detailed structural and magnetic studies are in agreement with the presence of abrupt spin crossover (*SCO*) behaviors and thermochromism in both derivatives.

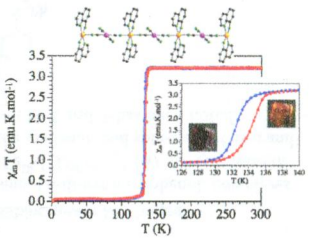

105 S dx.doi.org/10.1021/ic401747n

New [ONOO]-Type Amine Bis(phenolate) Ytterbium(II) and -(III) Complexes: Synthesis, Structure, and Catalysis for Highly Heteroselective Polymerization of *rac*-Lactide

Sheng Yang, Kun Nie, Yong Zhang, Mingqiang Xue, Yingming Yao, and Qi Shen*

Two divalent ytterbium (Yb^{II}) complexes, **1** and **2**, supported by new [ONOO]-type amine bis(phenolate) ligands $L^{a,b}$ were synthesized by an amine elimination reaction of $Yb^{II}(N(SiMe_3)_2)_2(TMEDA)$ (TMEDA = tetramethylethylenediamine) with one equivalent of the ligand precursor. Two new trivalent ytterbium (Yb^{III}) aryloxide complexes, **4** and **5**, bearing [ONOO]-type amine bis(phenolate) ligands L^c and L^d were prepared by double-protonation reaction of $Yb(C_5H_5)_3THF$ with one equivalent of the ligand precursor, then one equivalent of phenol. Complexes **1** and **4** were found to be extremely active for controlled ROP of *rac*-LA. Complexes **1**, **4** and **5** exhibited high stereoselectivity to give heterotactic polylactide with P_r ranging from 0.97 to 0.99.

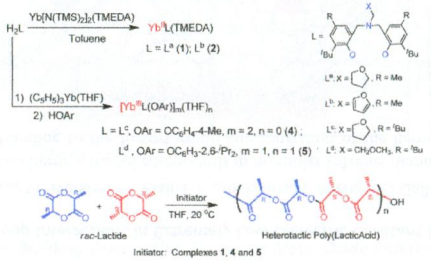

116 S dx.doi.org/10.1021/ic401753y

Syntheses, Crystal Structures, and Magnetic Properties of Four New Cyano-Bridged Bimetallic Complexes Based on the *mer*-$[Fe^{III}(qcq)(CN)_3]^-$ Building Block

Xiaoping Shen,* Hongbo Zhou, Jiahao Yan, Yanfeng Li, and Hu Zhou

Four cyano-bridged $Mn^{III/II}$ based complexes **1**–**4** constructed from *mer*-$[Fe^{III}(qcq)(CN)_3]^-$ have been synthesized and characterized. Complexes **1** and **2** feature a novel 1-D linear chain structure, while **3** and **4** are hexanuclear and trinuclear clusters. Slow magnetic relaxations are found for **1** and **2** at low temperature.

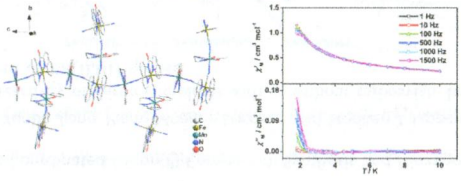

128 S dx.doi.org/10.1021/ic401755m

Deep Red Phosphorescence of Cyclometalated Iridium Complexes by *o*-Carborane Substitution

Hye Jin Bae, Jin Chung, Hyungjun Kim, Jihyun Park, Kang Mun Lee, Tae-Wook Koh, Yoon Sup Lee, Seunghyup Yoo,* Youngkyu Do,* and Min Hyung Lee*

The introduction of an *o*-carborane to the 4- or 5-position of the pyridine ring of a btp ligand in heteroleptic $(C^N)_2Ir(acac)$ complexes leads to deep red phosphorescence, which is substantially red-shifted compared to that of $(btp)_2Ir(acac)$. The solution processed PhOLED devices incorporating the 5-carborane substituted Ir(III) complex as an emitter display moderate performance with deep red phosphorescence.

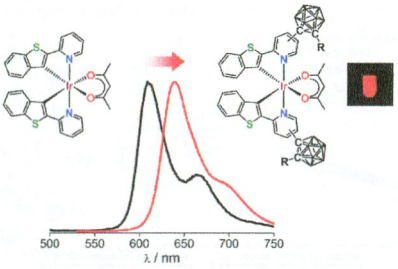

139 S dx.doi.org/10.1021/ic401762z

Probing Hydrogen Bond Networks in Half-Sandwich Ru(II) Building Blocks by a Combined ^{1}H DQ CRAMPS Solid-State NMR, XRPD, and DFT Approach

Michele R. Chierotti, Roberto Gobetto,* Carlo Nervi, Alessia Bacchi, Paolo Pelagatti, Valentina Colombo, and Angelo Sironi*

XRPD and SS NMR are complementary techniques providing long and short-range information, respectively, which can be further refined by DFT periodic lattice calculations. This combined approach has allowed us to shed light on the qualitative phase diagram of the $[(p\text{-cymene})Ru(\kappa N\text{-INA})Cl_2]$ polymorphic system (where INA is isonicotinic acid) and to fully characterize the changes in the hydrogen bond networks inherent to all of these phase transformations.

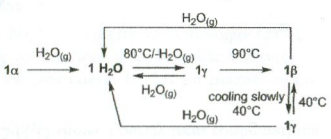

147 S dx.doi.org/10.1021/ic401801u

$La_{10}W_2O_{21}$: An Anion-Deficient Fluorite-Related Superstructure with Oxide Ion Conduction

Marie-Hélène Chambrier,* Armel Le Bail, Fabien Giovannelli, Abdelkrim Redjaïmia, Pierre Florian, Dominique Massiot, Emmanuelle Suard, and François Goutenoire

The crystal structure of $La_{10}W_2O_{21}$ is best described, on average, by a $2 \times 2 \times 2$ anion-deficient fluorite-related superstructure cubic cell, with space group $F\bar{4}_3m$, $Z = 4$, and $a = 11.17932(6)$ Å, similar to $Y_7ReO_{14-\delta}$. It is shown that classical cubic twinning along the 3-fold axis does take place. This compound exhibits interesting fast oxide ion conducting properties, comparable with LAMOX at low temperature.

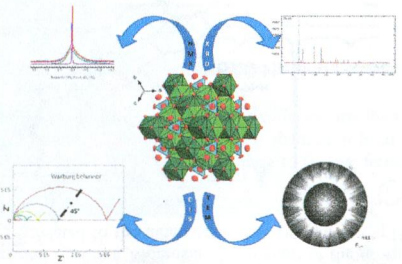

160 S dx.doi.org/10.1021/ic402614w

Ruthenium(II) Tris(2,2′-bipyridine)-Templated Zinc(II) 1,3,5-Tris(4-carboxyphenyl)benzene Metal Organic Frameworks: Structural Characterization and Photophysical Properties

Christi L. Whittington, Lukasz Wojtas, and Randy W. Larsen*

Here the ability of Ru(II) tris(2,2′-bipyridine) cations to template two new MOF structures from Zn(II) ions and 1,3,5-tris(4-carboxyphenyl)benzene tribenzoic acid is presented. The new MOFs impart novel photophysical properties to the encapsulated Ru(II) bipyridine complex. Of key interest is that encapsulation appears to populate new electronic excited states within the Ru(II) complex.

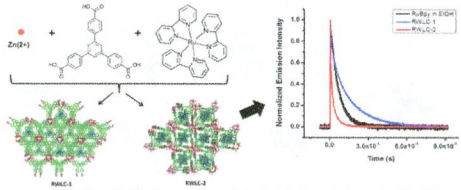

167 S dx.doi.org/10.1021/ic4019585

Versatile Reactivity of a Solvent-Coordinated Diiron(II) Compound: Synthesis and Dioxygen Reactivity of a Mixed-Valent $Fe^{II}Fe^{III}$ Species

Amit Majumdar, Ulf-Peter Apfel, Yunbo Jiang, Pierre Moënne-Loccoz,* and Stephen J. Lippard*

Synthesis, characterization, and reactivity of diiron complexes with or without carboxylate bridges, featuring reversible dioxygen activity of a mixed-valent diiron(II,III) species.

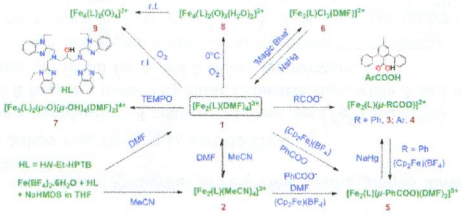

182 S dx.doi.org/10.1021/ic401986n

Evaluation of Heme Peripheral Group Interactions in Extremely Low-Dielectric Constant Media and Their Contributions to the Heme Reduction Potential.

Jose F. Cerda,* Mary C. Malloy, Brady O. Werkheiser, Alaina T. Stockhausen, Michael F. Gallagher, and Andrew C. Lawler

Electrochemical studies of heme *b* and heme *a* model compounds in nonpolar solvents demonstrate that the heme *a* reduction potential can be modulated by H-bonding to the formyl group and ionization of the heme propionates.

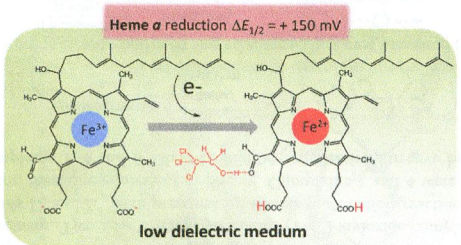

189 dx.doi.org/10.1021/ic402036p

Synthesis, Characterization, And Computational Study of Complexes Containing Pt···H Hydrogen Bonding Interactions

Miguel Baya, Úrsula Belío, and Antonio Martín*

Platinum(II) complexes containing hydroxyquinoline ligands show an intramolecular hydrogen bond in which the metal center acts as the proton acceptor, both in the solid state (X-ray) and in solution (NMR). Computational studies indicate that this bond is electrostatic but with a *partial covalence*. Moreover, the amount of the downfield displacement of the ^{1}H NMR signal (typical for hydrogen bonding) is related to the difference in the charges of the H and Pt atoms.

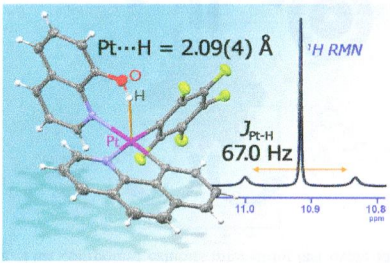

201 dx.doi.org/10.1021/ic402096s

Spin-Crossover Behavior in Two New Supramolecular Isomers

Zheng Yan, Zhao-Ping Ni, Fu-Sheng Guo, Jin-Yan Li, Yan-Chong Chen, Jun-Liang Liu, Wei-Quan Lin, Daniel Aravena, Eliseo Ruiz,* and Ming-Liang Tong*

Two spin-crossover (SCO) supramolecular isomers formulated as $[Fe(Mebpt)\{Au(CN)_2\}]_n \cdot xH_2O$ have been successfully isolated. Compound **1** is a two-dimensional coordination layer with both *cis* and *trans* octahedral configurations, in which only the Fe(II) centers in *trans* configuration exhibit spin transition (T_c = 303 K), while **2**·H_2O showed purely *trans* configurations undergoing two-step SCO.

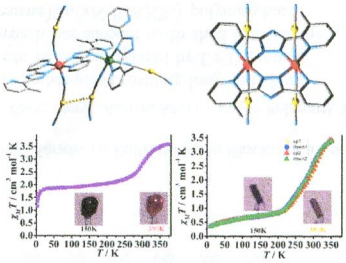

209 S dx.doi.org/10.1021/ic402128c

Geometrical Spin Frustration and Ferromagnetic Ordering in $(Mn_xPb_{2-x})Pb_2Sb_4Se_{10}$

Pierre F. P. Poudeu,* Honore Djieutedjeu, Kulugammana G. S. Ranmohotti, Julien P. A. M. Makongo, and Nathan Takas

Isomorphic substitutions of Pb^{2+} by Mn^{2+} within the $[Pb_6Se_{30}]_\infty$ cluster in the structure of $Pb_4Sb_4Se_{10}$ generate quasi-isolated one-dimensional $[(Mn_xPb_{2-x})_3Se_{30}]$ magnetic subunits with geometrically frustrated spin distributions coherently embedded within the semiconducting main-group metal selenide framework. At a critical temperature of 125 K, moments within individual magnetic subunits undergo cooperative ferromagnetic ordering leading to exceptionally high effective magnetic moment.

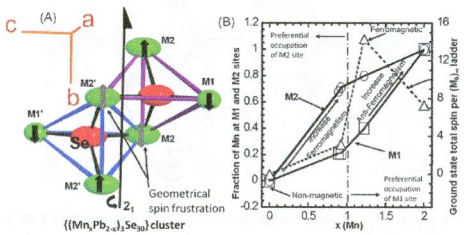

221 S dx.doi.org/10.1021/ic402177j

Polar Alignment of Λ-Shaped Basic Building Units within Transition Metal Oxide Fluoride Materials

Michael Holland, Martin D. Donakowski, Eric A. Pozzi, Andrew M. Rasmussen, Thanh Thao Tran, Shannon E. Pease-Dodson, P. Shiv Halasyamani, Tamar Seideman, Richard P. Van Duyne, and Kenneth R. Poeppelmeier*

A series of pseudosymmetrical structures of formula $K_{10}(M_2O_nF_{11-n})_3X$ (M = V and Nb, n = 2, X = $(F_2Cl)_{1/3}$, Br, $Br_{4/2}I_{4/2}$; M = Mo, n = 4, X = Cl, $Br_{4/2}$, $I_{4/2}$) illustrates generation of polar structures with the use of Λ-shaped basic building units (BBUs). These materials differ in their (non)centrosymmetry despite chemical and structural similarities. These Λ-shaped BBUs form as a consequence of the coordination environment around the bridging anion of the metal oxide fluoride BBUs.

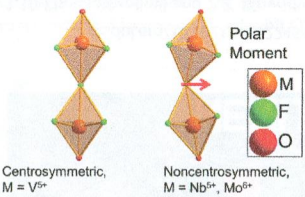

229 S dx.doi.org/10.1021/ic402187e

Proton-Induced Reversible Modulation of the Luminescent Output of Rhenium(I), Iridium(III), and Ruthenium(II) Tetrazolate Complexes

Melissa V. Werrett, Sara Muzzioli, Phillip J. Wright, Antonio Palazzi, Paolo Raiteri, Stefano Zacchini, Massimiliano Massi,* and Stefano Stagni*

Tetrazolate-based complexes are electrophile-sensitive molecules. In particular, protonation reaction causes dramatic changes in the luminescent performances of Re(I), Ir(III), and Ru(II) tetrazolate complexes. Taking advantage of the use of a protonation–deprotonation protocol, it is therefore possible to reversibly modulate the luminescence output of such metal tetrazolate complexes.

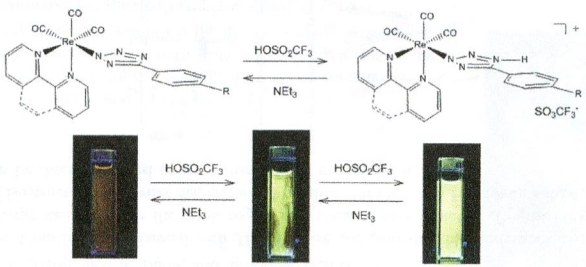

244 dx.doi.org/10.1021/ic402200v

Synthesis, Crystal Structures, Magnetic, and Thermal Properties of Divalent Metal Formate–Formamide Layered Compounds.

Pradeep Samarasekere, Xiqu Wang, Allan J. Jacobson,* Joshua Tapp, and Angela Möller*

A series of layered metal formate compounds, $[M(HCOO)_2(HCONH_2)_2]$ (M = Mn, Ni, Cu, Zn, Mg) were obtained by solvothermal reactions of divalent metal salts with. The compounds consist of $M(HCOO)_2$ layers with formamide ligands coordinated to the metal centers acting as spacers between the layers. The Mn, Ni, and Zn compounds show order–disorder phase transformations associated with the formamide $-NH_2$ groups. The magnetic properties of the Mn, Ni, and Cu compounds are dominated by antiferromagnetic exchange interactions.

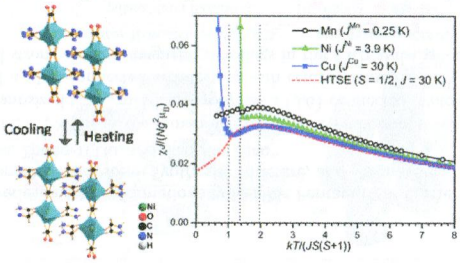

257 dx.doi.org/10.1021/ic4022068

Strong and Anisotropic Superexchange in the Single-Molecule Magnet (SMM) $[Mn^{III}_6Os^{III}]^{3+}$: Promoting SMM Behavior through 3d–5d Transition Metal Substitution

Veronika Hoeke, Anja Stammler, Hartmut Bögge, Jürgen Schnack,* and Thorsten Glaser*

Substitution of the 3d ion Fe^{III} l.s. in $[\mathbf{Mn^{III}_6Fe^{III}}]^{3+}$ (= $[\{(talen^{t\text{-}Bu_2})Mn^{III}_3\}_2\{Fe^{III}(CN)_6\}]^{3+}$) with its 5d homologue Os^{III} l.s. leads to a strengthening of the $M^{central}$–Mn^{III} exchange interaction along with the manifestation of an Ising-like exchange anisotropy. As a consequence, the single-molecule magnet $[\mathbf{Mn^{III}_6Os^{III}}]^{3+}$ exhibits a higher energy barrier for magnetization reversal than $[\mathbf{Mn^{III}_6Fe^{III}}]^{3+}$.

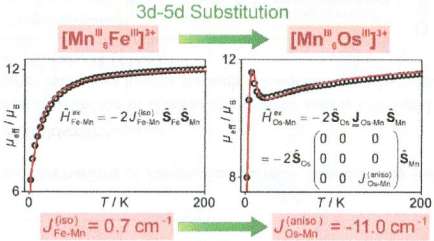

269 dx.doi.org/10.1021/ic402210j

Multiple, Disparate Redox Pathways Exhibited by a Tris(pyrrolido)ethane Iron Complex

Graham T. Sazama and Theodore A. Betley*

Iron(II) bound to the trianionic trispyrrolyl ligand (tpe), and two redox pathways are observed. Outer-sphere electron-transfer is dominated by the high-lying tpe-ligand π-orbitals, leading to H-atom abstraction from a ligand-based radical. Oxidation occurring via an inner-sphere electron transfer is metal centered, leading to anionic ferric complexes.

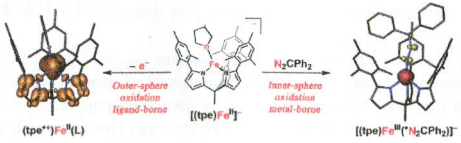

282 S dx.doi.org/10.1021/ic4022239

Tuning the Host–Guest Interactions in a Phosphine Coordination Polymer through Different Types of *post*-Synthetic Modification

Ana J. Nuñez, Maxwell S. Chang, Ilich A. Ibarra, and Simon M. Humphrey*

PCM-10 is a Phosphine Coordination Material with 3D structure and porosity that undergoes a series of *post*-synthetic modifications at the phosphine sites inside the pores to generate unusual pore moieties (P–AuCl, P=O, and $[P–CH_3]^+ X^-$). The resulting family of isostructural materials display broad tunability in CO_2 and H_2 uptake behavior; the measured isosteric heats of adsorption can be directly related to the nature of the modification.

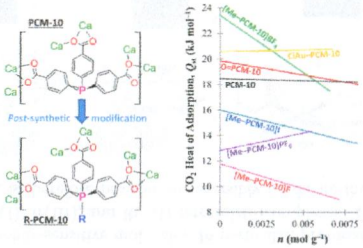

289 S dx.doi.org/10.1021/ic402228g

Color Tuning and White Light Emission via in Situ Doping of Luminescent Lanthanide Metal–Organic Frameworks

Qun Tang, Shuxia Liu,* Yiwei Liu, Danfeng He, Jun Miao, Xingquan Wang, Yujuan Ji, and Zhiping Zheng*

Lanthanide ion centers with identical coordination environment in lanthanide metal–organic frameworks prompt us to prepare mixed lanthanide analogues by way of in situ doping. With adjustment of the relative concentration of the lanthanide ions, tunable color and white light emission can be achieved.

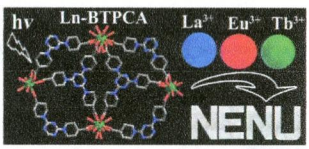

294 S dx.doi.org/10.1021/ic4022454

Ruthenium Bis-diimine Complexes with a Chelating Thioether Ligand: Delineating 1,10-Phenanthrolinyl and 2,2′-Bipyridyl Ligand Substituent Effects

Nathir A. F. Al-Rawashdeh, Sayandev Chatterjee, Jeanette A. Krause, and William B. Connick*

Ruthenium(II) diimine complexes with the π-acidic bidentate 1,2-bis(phenylthio)ethane (dpte) ligand exhibit surprising luminescence in room-temperature fluid solution. Variations in the MLCT energies and Ru(III/II) redox couple can be understood in terms of the influence of the donor properties of the ligands on the mainly metal-based HOMO and mainly diimine ligand-based LUMO. Analysis of the spectroscopic and electrochemical properties revealed surprising correlations and yielded recommended Hammett and electrochemical parametrizations for 2,2′-bipyridyl and 1,10′-phenanthrolinyl ligand substituents.

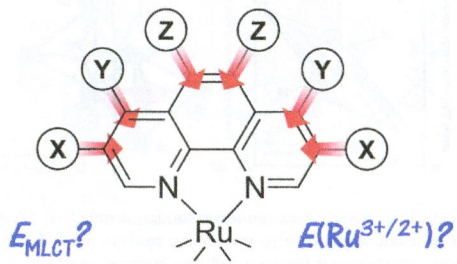

308 dx.doi.org/10.1021/ic402246d

Element Misidentification in X-ray Crystallography: A Reassessment of the [MCl_2(diazadiene)] (M = Cr, Mo, W) Series

Angelique F. Greene, P. Chandrasekaran, Yong Yan, Joel T. Mague, and James P. Donahue*

A reassessment of reported [MCl_2(diazadiene)] (M = Cr, Mo, W) complexes in the context of known chemistry of low-valent Group VI metal complexes, crystallographic trends such as M–Cl bond lengths and unit cell volumes, and calculated metal–ligand bond lengths points toward their formulation being incorrect. The CIFs accompanying the published structures show partial site occupancy factors for Mo (0.775) and W (0.4005, 0.417), which engender behavior as zinc, the metal atoms' true identity.

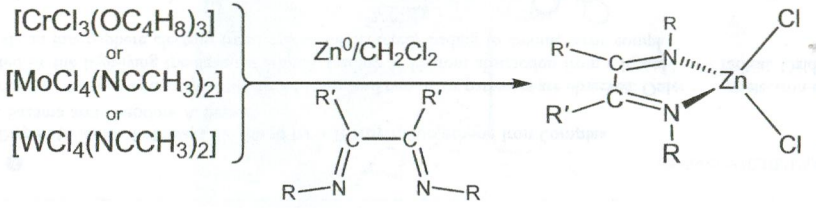

318 dx.doi.org/10.1021/ic402261v

Computational Examination of the Mechanism of Alkene Epoxidation Catalyzed by Gallium(III) Complexes with N-Donor Ligands

Michael L. McKee* and Christian R. Goldsmith*

The mechanism of gallium-catalyzed epoxidation of alkenes by peracetic acid is calculated to proceed through an electophilic κ^2 peracetate complex. The precatalyst exchanges ligands through a dissociative mechanism. The gallium in the reaction mostly exists as $[Ga(phen)_2(OAc)]^{2+}$ and $[Ga(phen)_2(OAc)_2]^{+}$.

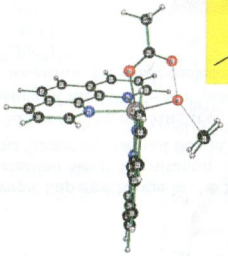

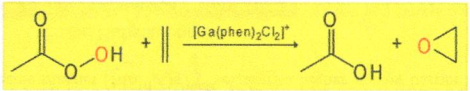

Reactivity proceeds through an electrophilic hexacoordinate Ga(III) species with a bidentate peracetate ligand

327 dx.doi.org/10.1021/ic402280p

Diverse Self-Assembly from Predesigned Conformationally Flexible Pentanuclear Clusters Observed in a Ternary Copper(II)–Triazolate–Sulfoisophthalate System: Synthesis, Structure, and Magnetism

En-Cui Yang,* Yuan-Yuan Zhang, Zhong-Yi Liu, and Xiao-Jun Zhao*

Self-assembly from predesigned Cu^{II}_5 SBUs in the ternary Cu^{II}–triazolate–sulfoisophthalate system respectively generates a pillared-layer framework with nanosized Cu^{II}_{30} metallamacrocycles, a (3,6)-connected twofold interpenetrating topological net with Cu^{II}_5 and Cu^{II}_1 cores, and a (4,8)-connected architecture with centrosymmetric Cu^{II}_7 clusters, which exhibit field-dependent metamagnetism and strong antiferromagnetic couplings in the Cu^{II}_5 and Cu^{II}_7 cores.

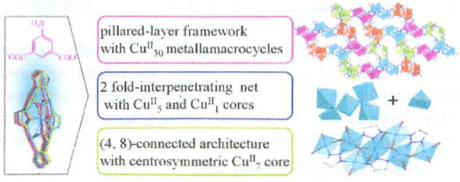

336 dx.doi.org/10.1021/ic402283c

Crystal-Chemistry Guidelines for Noncentrosymmetric A_2BO_4 Ruddlesden–Popper Oxides

Prasanna V. Balachandran, Danilo Puggioni, and James M. Rondinelli*

Materials without inversion symmetry are critical for many technological applications. We examine the two-dimensional A_2BO_4 Ruddlesden–Popper oxides, which remarkably have a strong preference to centrosymmetric geometries. Using representation theory, materials informatics, and density functional theory calculations, we uncover the underlying structural constraints on inversion symmetry to formulate predictive inversion symmetry lifting structure and cation selection guidelines. Cation order and/or multiple octahedral distortions are found to be viable routes; the latter tested in divalent iridates.

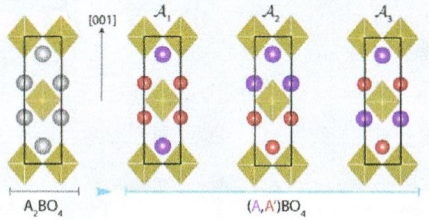

349 dx.doi.org/10.1021/ic4022917

Doping the Alkali Atom: An Effective Strategy to Improve the Electronic and Nonlinear Optical Properties of the Inorganic $Al_{12}N_{12}$ Nanocage

Min Niu, Guangtao Yu,* Guanghui Yang, Wei Chen,* Xingang Zhao, and Xuri Huang*

Doping the alkali atom can be a simple and effective strategy to improve the electronic and nonlinear optical (NLO) properties of inorganic AlN nanocages, and endow them with the intriguing *n*-type characteristic and large second-order NLO response as well as the excellent stability.

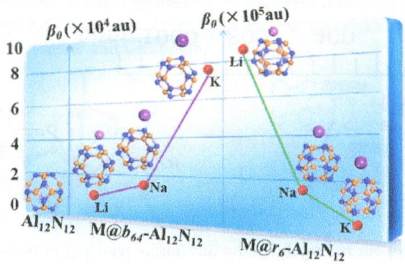

359 dx.doi.org/10.1021/ic402292a

Solution-Chemical Route to Generalized Synthesis of Metal Germanate Nanowires with Room-Temperature, Light-Driven Hydrogenation Activity of CO_2 into Renewable Hydrocarbon Fuels

Qi Liu, Yong Zhou,* Wenguang Tu, Shicheng Yan, and Zhigang Zou*

A facile solution-chemical route was developed for the generalized preparation of a series of metal germanate nanowires on a large scale, which is based on the use of hydrazine monohydrate as an alkali solvent, coordination agent, and anisotropic crystal growth director under solvothermal conditions.

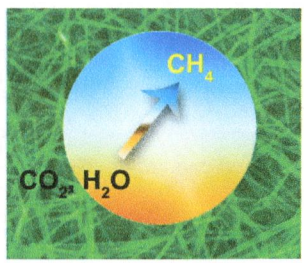

365 S dx.doi.org/10.1021/ic402294g

Synthesis and Characterization of the Crystal and Magnetic Structures and Properties of the Hydroxyfluorides Fe(OH)F and Co(OH)F

Hamdi Ben Yahia,* Masahiro Shikano,* Mitsuharu Tabuchi, Hironori Kobayashi, Maxim Avdeev, Thiam Teck Tan, Samuel Liu, and Chris D. Ling

The title compounds crystallize with structures related to the diaspore-type α-AlOOH. The protons are located in the channels and form O−H···F *bent* hydrogen bonds. The magnetic susceptibility data for the cobalt phase indicate antiferromagnetic ordering below ~40 K, and the neutron powder diffraction measurements at 3 K show that ferromagnetic rutile-type chains with spins parallel to the *b* axis are antiferromagnetically coupled to each other, similarly to the magnetic structure of goethite α-FeOOH.

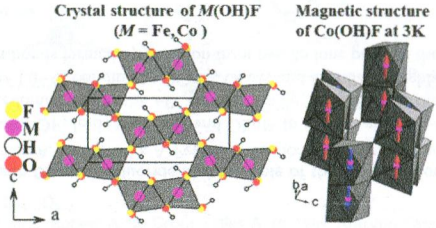

375 S dx.doi.org/10.1021/ic402306c

A ^{23}Na Magic Angle Spinning Nuclear Magnetic Resonance, XANES, and High-Temperature X-ray Diffraction Study of $NaUO_3$, Na_4UO_5, and $Na_2U_2O_7$

A. L. Smith,* P. E. Raison,* L. Martel, T. Charpentier, I. Farnan, D. Prieur, C. Hennig, A. C. Scheinost, R. J. M. Konings, and A. K. Cheetham

X-ray absorption near edge structure (XANES) studies performed on $NaUO_3$, Na_4UO_5, and $Na_2U_2O_7$ have confirmed the valence state of uranium in those compounds, namely V, VI, and VI, respectively. Solid-state ^{23}Na magic angle spinning nuclear magnetic resonance (MAS NMR) measurements have also evidenced a paramagnetic shift in $NaUO_3$, which has the electronic structure $[Rn](5f^1)$. NMR parameters have been estimated on the $[Rn](5f^0)$ systems using DFT calculations and found to be in good agreement with experiment.

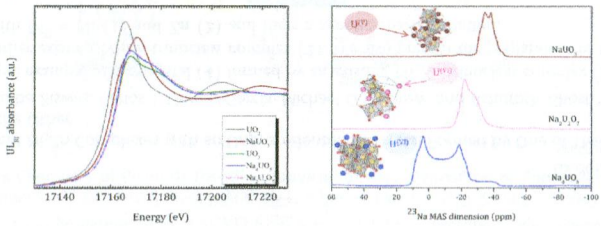

XANES spectra *MAS-NMR*

383 S dx.doi.org/10.1021/ic4023294

Supramolecular Interactions in $PuO_2Cl_4^{2-}$ and $PuCl_6^{2-}$ Complexes with Protonated Pyridines: Synthesis, Crystal Structures, and Raman Spectroscopy

Richard E. Wilson,* David D. Schnaars, Michael B. Andrews, and C. L. Cahill*

Plutonyl tetrachloride anions are assembled through protonated amines. Crystal structures and Raman spectra are reported.

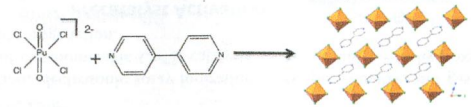

393 dx.doi.org/10.1021/ic402346z

Regioisomer-Dependent Endo- and Exocyclic Coordination of Bis-Dithiamacrocycles

Arlette Deukam Siewe, Ja-Yeon Kim, Seulgi Kim, In-Hyeok Park, and Shim Sung Lee*

Syntheses of the regioisomers of bis-dithiamacrocycle and the regioisomer-controlled endo- and exocyclic coordination behaviors are reported.

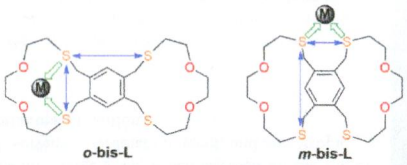

399 dx.doi.org/10.1021/ic402354r

Solid State ^{13}C and ^{2}H NMR Investigations of Paramagnetic [Ni(II)(acac)$_2$L$_2$] Complexes

Anders Lennartson, Lene Ulrikke Christensen, Christine J. McKenzie, and Ulla Gro Nielsen*

Solid state ^{13}C MAS NMR spectroscopy has been used to investigate nine paramagnetic [Ni(II)(acac)$_2$L$_2$] complexes with L = H_2O, D_2O, NH_3, MeOH, $PMePh_2$, PMe_2Ph, and [dppe]$_{1/2}$. Characteristic values for $\delta(^{13}C)$ and the anisotropy are observed for the ligands. The ^{13}C NMR spectra of three phosphines with L = $PPhMe_2$, PPh_2Me, and dppe were assigned using these correlations. The CSA is a large fraction of the total anisotropy especially for the methine (CH) in the acac$^-$ ligand.

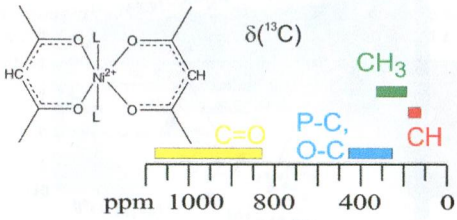

409 dx.doi.org/10.1021/ic402387b

Synthesis and Photochemical Properties of pH Responsive Tris-Cyclometalated Iridium(III) Complexes That Contain a Pyridine Ring on the 2-Phenylpyridine Ligand

Akihiro Nakagawa, Yosuke Hisamatsu, Shinsuke Moromizato, Masahiro Kohno, and Shin Aoki*

The design and synthesis of new cyclometalated Ir(III) complexes having three pyridyl groups at the 5′-position of the ligands (Ir(4Pyppy)$_3$, Ir(3Pyppy)$_3$, Ir(4Pyppym)$_3$, Ir(3Pyppym)$_3$) are reported. The strong green emission of Ir(4Pyppy)$_3$ and Ir(4Pyppym)$_3$ exhibited a significant red-shift upon the protonation of the three pyridine rings, which is opposite behavior to that of *fac*-Ir(atpy)$_3$ containing three amino groups at the same position. Staining and photoirradiated cell death of HeLa-S3 cells by the use of Ir(4Pyppy)$_3$ are also reported.

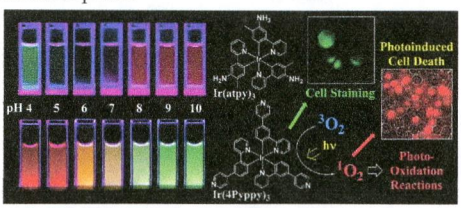

423 S dx.doi.org/10.1021/ic402390t

Modes of Activation of Organometallic Iridium Complexes for Catalytic Water and C–H Oxidation

Andrew J. Ingram, Arron B. Wolk, Cornelia Flender, Jialing Zhang, Christopher J. Johnson, Ulrich Hintermair, Robert H. Crabtree, Mark A. Johnson,* and Richard N. Zare*

Desorption electrospray ionization, electrosonic spray ionization mass spectrometry, and gas-phase IR spectroscopy of ions detected during the activation of organometallic Cp*Ir catalysts for water and C–H hydroxylation indicate a complex, nonselective mechanism for Cp* oxygenation.

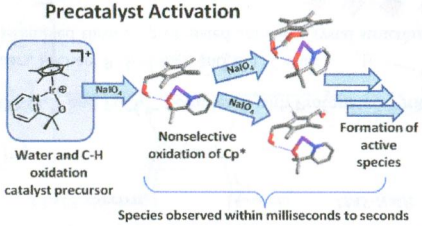

434 S dx.doi.org/10.1021/ic402415b

Isolation of Two Different Ni_2Zn Complexes with an Unprecedented Cocrystal Formed by One of Them and a "Coordination Positional Isomer" of the Other

Lakshmi Kanta Das, Apurba Biswas, Carlos J. Gómez-García, Michael G. B. Drew, and Ashutosh Ghosh*

Here we present a unique example of a cocrystal (**4**) formed by an existing Ni_2Zn trinuclear complex (**3**) and a "coordination position isomer" of another existing Ni_2Zn trinuclear complex (**2**). We also present the preparation of two isostructural Ni_2M trinuclear complexes with M^{II} = Ni (**1**) and Zn (**2**) and their magnetic characterization.

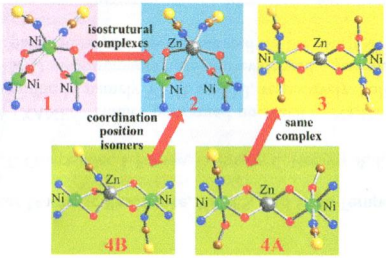

446 S dx.doi.org/10.1021/ic402422h

Reactions of Lanthanide Atoms with Oxygen Difluoride and the Role of the Ln Oxidation State

Tanya Mikulas, Mingyang Chen, David A. Dixon,* Kirk A. Peterson, Yu Gong, and Lester Andrews*

The reaction of lanthanide atoms with OF_2 leads to $OLnF_2$ and OLnF. In $OLnF_2$, except for Ln = Ce, Pr, and Tb which are predominantly in the +IV oxidation state, the Ln are in the +III state as they are in OLnF. The Ln–O bonding in $OCeF_2$, OLaF, and OLuF is a highly polarized σ bond and two pseudo π bonds formed by donation from two 2p lone pairs on the O to the Ln.

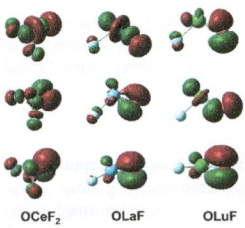

457 S dx.doi.org/10.1021/ic402425n

Order–Disorder Transition and Weak Ferromagnetism in the Perovskite Metal Formate Frameworks of $[(CH_3)_2NH_2][M(HCOO)_3]$ and $[(CH_3)_2ND_2][M(HCOO)_3]$ (M = Ni, Mn)

Mirosław Mączka,* Anna Gągor, Bogusław Macalik, Adam Pikul, Maciej Ptak, and Jerzy Hanuza

We report the synthesis and temperature-dependent studies of $[(CH_3)_2ND_2][M(HCOO)_3]$ and $[(CH_3)_2NH_2][M(HCOO)_3]$ formates (M = Ni, Mn). These compounds undergo a first-order phase transition accociated with ordering of DMA^+ cations. Some amount of motion is retained by the DMA^+ cation in the ferroelectric phase, and a complete freezing-in of this motion occurs below 100 K. Weak anomalies in the temperature dependence of vibrational frequencies below 40 K are attributed to spin-phonon coupling.

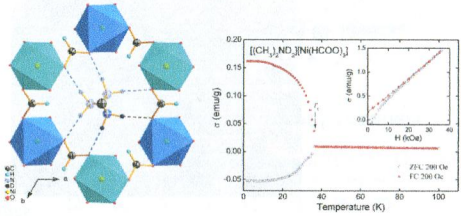

468 S dx.doi.org/10.1021/ic4024508

Triamidetriamine Bearing Macrobicyclic and Macrotricyclic Ligands: Potential Applications in the Development of Copper-64 Radiopharmaceuticals

Kel Vin Tan, Paul A. Pellegrini, Brian W. Skelton, Conor F. Hogan, Ivan Greguric, and Peter J. Barnard*

Triamide bearing analogues of sarcophagine hexaazamacrobicyclic cage ligands were prepared without the need for a templating metal ion. The Co(III) and Cu(II) complexes for one cryptand (7) were synthesized, and these compounds displayed octahedral and square planar coordination geometries, respectively. These cryptands are of interest for radiopharmaceutical applications, cryptand 7 was labeled with ^{64}Cu and this complex showed good stability when challenged with the metal binding amino acids, L-cysteine and L-histidine.

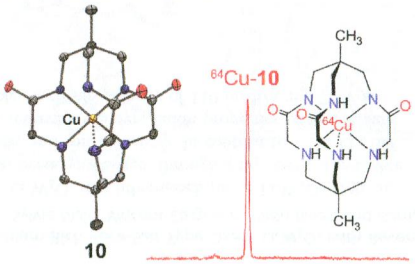

478 dx.doi.org/10.1021/ic4024663

New Approach to Tolman's Electronic Parameter Based on Local Vibrational Modes

Robert Kalescky, Elfi Kraka, and Dieter Cremer*

Tolman's electronic parameter (TEP) is improved by replacing normal with local CO stretching frequencies because the former are always flawed by mode–mode coupling. Local TEP (LTEP) values are based on local CO stretching force constants and, therefore, no longer suffer from mode coupling and mass effects. The LTEP values of 42 nickel complexes of the type $LNi(CO)_3$ lead to a different ordering of ligand electronic effects than the corresponding TEP values.

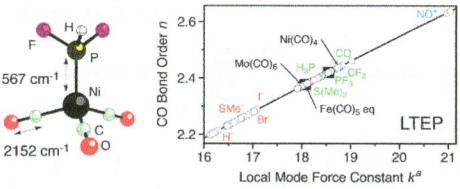

496 dx.doi.org/10.1021/ic402493q

Anionogenic Mixed Valency in $K_xBa_{1-x}O_{2-\delta}$

Shivakumara Giriyapura, Baomin Zhang, Robert A. de Groot, Gilles A. de Wijs, Antonio Caretta, Paul H. M. van Loosdrecht, Winfried Kockelmann, Thomas T. M. Palstra, and Graeme R. Blake*

Members of the novel solid solution series $K_xBa_{1-x}O_{2-\delta}$ exhibit four oxygen–oxygen stretching modes in their Raman spectra. These modes do not arise from individual dioxygen anions, but rather from in-phase and anti-phase coupling of the stretching of anions that have mixed coordinations of K^+ and Ba^{2+}. This coupling is a direct signature of the mixed-valent nature of these compounds.

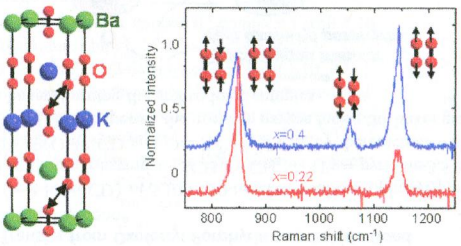

503 dx.doi.org/10.1021/ic402499r

Synthesis and Materials Chemistry of Bismuth *Tris*-(di-i-propylcarbamate): Deposition of Photoactive Bi_2O_3 Thin Films

Samuel D. Cosham, Michael S. Hill, Graeme A. Horley, Andrew L. Johnson, Laura Jordan, Kieran C. Molloy,* and David C. Stanton

δ- and β-Bi_2O_3 thin films can be deposited by AACVD from a $Bi(O_2CNPr^i_2)_3$ precursor, with temperature and temporal control over the deposition process. Thin δ-Bi_2O_3 films show good catalytic activity toward the photodegradation of methylene blue, while β-Bi_2O_3 nanowires are less active because of an increased hydrophobicity. Controlled hydrolysis of $Bi(O_2CNPr^i_2)_3$ affords the novel oxo-cluster $Bi_8(O)_6(O_2CNPr^i_2)_{12}$.

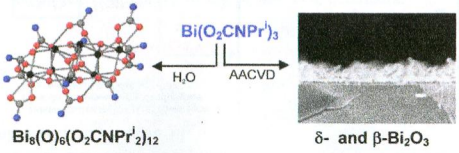

512 Ⓢ dx.doi.org/10.1021/ic402533j

Computational Insights on the Geometrical Arrangements of Cu(II) with a Mixed-Donor N_3S_3 Macrobicyclic Ligand

Andrés G. Algarra,* Gabriel Aullón, Paul V. Bernhardt, and Manuel Martínez

On the basis of a computational study and previously reported experimental data, a mechanism is proposed for the interconversion between hexadentate (N_3S_3, Cu-in^{2+}) and tetradentate (N_2S_2, Cu-out^{+}) Cu(II) complexes of AMME-N_3S_3sar as well as the effect of solvent on their relative stability.

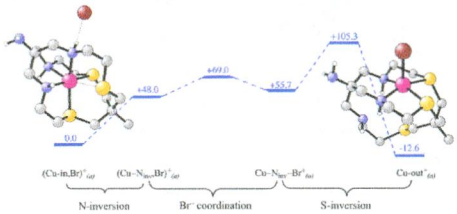

522 dx.doi.org/10.1021/ic402543e

Electrochemical Synthesis of a Lithium-Rich Rock-Salt-Type Oxide $Li_5W_2O_7$ with Reversible Deintercalation Properties

Valerie Pralong,* Gopal Venkatesh, Sylvie Malo, Vincent Caignaert, Radu Baies, and Bernard Raveau

Starting from the ribbon structure $Li_2W_2O_7$, the lithium-rich phase $Li_5W_2O_7$ with an ordered rock-salt-type structure has been synthesized, through a topotactic irreversible reaction, using both electrochemistry and soft chemistry. In contrast to $Li_2W_2O_7$, the lithium-rich oxide $Li_5W_2O_7$ shows reversible deintercalation properties of two lithium molecules per formula unit: a stable reversible capacity of 110 mAh/g at 1.70 V is maintained after 20 cycles.

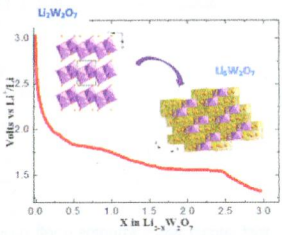

528 Ⓢ dx.doi.org/10.1021/ic402578m

Multidimensional Open-Frameworks: Combinations of One-Dimensional Channels and Two-Dimensional Layers in Novel Bi/M Oxo-Chlorides

Minfeng Lü, Almaz Aliev, Jacob Olchowka, Marie Colmont, Marielle Huvé, Claudia Wickleder, and Olivier Mentré*

Here we discuss the synthesis and characterization of three novel bismuth oxo-chlorides: $[Bi_6Na_{0.5}O_{7.5}][Na_{0.5}Cl_3]_{channel}[Cl]_{layer}$, $[Bi_{17}PbO_{22}][Cl_6]_{channel}[Cl_3]_{layer}$, and $[Bi_9(Pb_{0.2}Mn_{0.8})O_{12}][Cl_3]_{channel}$ $[Cl_2]_{layer}$ which all show an original multidimensional crystal structure. It is formed of 2D-layered blocks separated by Cl^- layers. The blocks are porous with triangular 1D-Cl^- channels with various section sizes.

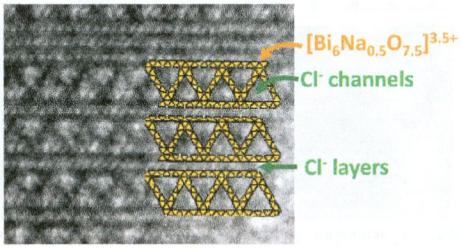

537 Ⓢ dx.doi.org/10.1021/ic402561g

From Solution to the Solid State: Control of Niobium Oxide–Fluoride $[NbO_xF_y]^{n-}$ Species

Hongcheng Lu, Romain Gautier, Martin D. Donakowski, Zhengtang Liu, and Kenneth R. Poeppelmeier*

The $[NbOF_4]^-$, $[NbOF_5]^{2-}$, and $[NbF_6]^-$ anions can be successively targeted in crystal structures by increasing the corresponding pK_a of the organic reagent. Infinite chains of $[NbOF_4]^-$ anions form when the corresponding pK_a of the organic base introduced ranges approximately between 3.17 and 7.14. In contrast, isolated $[NbOF_5]^{2-}$ anions form when the corresponding pK_a of the organic base introduced is approximately between 7.14 and 11, and $[NbF_6]^-$ forms when the corresponding pK_a of the organic molecule is above 11.

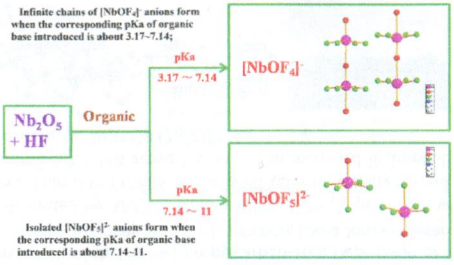

543 Ⓢ dx.doi.org/10.1021/ic4026393

Intramolecular Direct Oxygen Transfer from Oxoferryl Porphyrin to a Sulfide Bond

Takunori Ueda, Hiroaki Kitagishi, and Koji Kano*

A 1:1 supramolecular complex (met-hemoCD) of 5,10,15,20-tetrakis(4-sulfonatophenyl)porphyrinatoiron(III) (Fe^{III}TPPS) with per-*O*-methylated β-cyclodextrin dimer having a $-SCH_2Py\ CH_2S-$ (Py = pyridine-3,5-diyl) linker (Py3CD) formed two types of ferryloxo species, $O{=}Fe^{IV}P(OH^-)CD$ and $O{=}Fe^{IV}(Py)PCD$, by the reaction with hydroperoxide or cumene hydroperoxide. For the $O{=}Fe^{IV}(OH^-)PCD$ species, the iron-oxo oxygen facing the linker gradually and directly transferred to the nearby sulfide bond on the linker, forming the sulfoxidized complex.

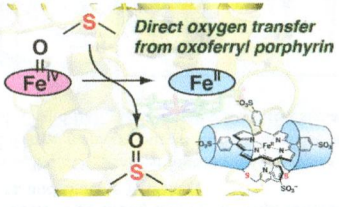

552 S dx.doi.org/10.1021/ic402658d

Alkaline-Earth Metal Carboxylates Characterized by ^{43}Ca and ^{87}Sr Solid-State NMR: Impact of Metal-Amine Bonding

Kevin M. N. Burgess, Yang Xu, Matthew C. Leclerc, and David L. Bryce*

Ultrahigh-field ^{43}Ca and ^{87}Sr solid-state NMR spectroscopies, which present various technical challenges, are applied to the study of a series of model organic Ca^{2+} and Sr^{2+} complexes. The spectral parameters are sensitive to the metal cations' coordination environments and, in particular, to the presence of nitrogen-containing functional groups in their first coordination spheres. Along with the experimental data, projector-augmented wave DFT computations provide insights into the relationship between the NMR parameters and the local structure.

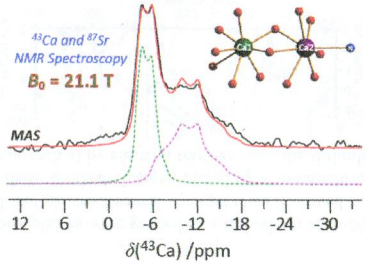

562 S dx.doi.org/10.1021/ic4026624

Calix[4]arene-Supported Mononuclear Lanthanide Single-Molecule Magnet

Feng Gao, Long Cui, You Song, Yi-Zhi Li, and Jing-Lin Zuo*

Three interesting single lanthanide-based complexes encapsulated by calix[4]arene and the Kläui's tripodal ligands have been synthesized and characterized. The dysprosium complex displays obvious SMM behavior with characteristic magnetic hysteresis loops and the slow relaxation of magnetization.

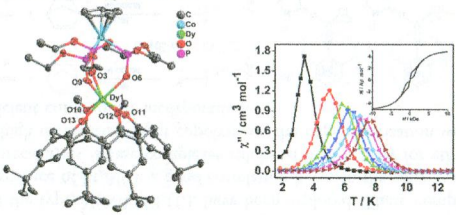

568 S dx.doi.org/10.1021/ic4026848

1′-(Diphenylphosphino)-1-cyanoferrocene: A Simple Ligand with Complicated Coordination Behavior toward Copper(I)

Karel Škoch, Ivana Císařová, and Petr Štěpnička*

The ferrocene-based phosphinonitrile [Fe(η^5-$C_5H_4PPh_2$)(η^5-C_5H_4CN)] has been explored as a donor in copper(I) complexes with and without supporting halide ligands. The course of the complexation reactions was found to depend on the copper source and the Cu/ligand ratio, leading to conventional products featuring the phosphinonitrile as a P-monodentate ligand as well as unprecedented complexes in which the ligand act as a P,N bridge employing both soft donor moieties. Compounds combining both coordination modes are also described.

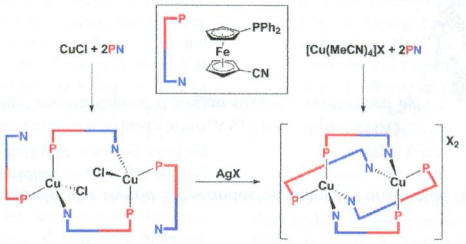

578 S dx.doi.org/10.1021/ic4027249

Two Novel Ternary Dicopper(II) μ-Guanazole Complexes with Aromatic Amines Strongly Activated by Quantum Dots for DNA Cleavage

Javier Hernández-Gil, Sacramento Ferrer,* Alfonso Castiñeiras, Malva Liu-González, Francesc Lloret, Ángela Ribes, Lucija Čoga, Anja Bernecker, and Juan C. Mareque-Rivas*

Two novel (μ-guanazole/ate)-bridged binuclear copper(II) complexes with 1,10-phenanthroline (phen) or 2,2′-bipyridine (bipy), [Cu_2(μ-*N*2,*N*4-Hdatrz)-$(phen)_2(H_2O)(NO_3)_4$] (**1**) and [Cu_2(μ-*N*1,*N*2-datrz)$_2$(μ-OH_2)$(bipy)_2$]$(ClO_4)_2$ (**2**) (Hdatrz = 3,5-diamino-1,2,4-triazole = guanazole), have been prepared and characterized by X-ray diffraction, spectroscopy, and susceptibility measurements [J ($\mu_{2,4}$-triazole) = −52 cm^{-1} for **1** and J ($\mu_{1,2}$-triazolate) = −115 cm^{-1} for **2**] and combined with quantum dots (QD) to develop efficient DNA-cleaving systems.

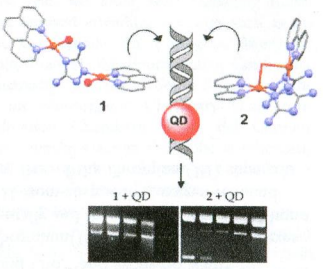

594 S dx.doi.org/10.1021/ic402740k

Order–Disorder Transition Involving the A-Site Cations in $Ln^{3+}Mn_3V_4O_{12}$ Perovskites

Yuichi Shimakawa,* Shoubao Zhang, Takashi Saito, Michael W. Lufaso, and Patrick M. Woodward

A crossover from the A-site-ordered double-perovskite structure with $Im\bar{3}$ cubic symmetry to the simple-perovskite structure with *Pnma* orthorhombic symmetry is found in $LnMn_3V_4O_{12}$ (*Ln* = La, Nd, Gd, Y, Lu). The observed phase crossover is a result of the structural stability due to the cooperative tilting of the VO_6 octahedra.

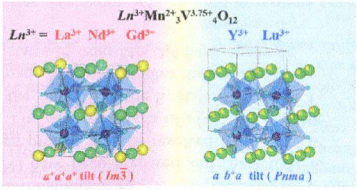

600 S dx.doi.org/10.1021/ic402742f

Aminotroponiminato(chloro)germylene Stabilized Copper(I) Iodide Complexes: Synthesis and Structure

Dhirendra Yadav, Rahul Kumar Siwatch, Soumen Sinhababu, and Selvarajan Nagendran*

Using an aminotroponiminato(chloro)germylene **1**, the first example of a germylene stabilized copper(I) iodide complex **3** with a monomeric CuI core is reported. Utilizing it further, two other copper(I) iodide complexes **2** and **4** with tetrameric Cu_4I_4 and dimeric Cu_2I_2 cores are also synthesized, respectively. Further, for the first time, an interesting interconversion between compounds **3** and **4** and the conversion of compound **2** to compounds **3** and **4** have been demonstrated.

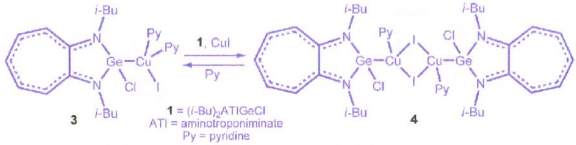

607 S dx.doi.org/10.1021/ic402747d

Synthesis and Structural Analysis of (Imido)vanadium(V) Dichloride Complexes Containing Imidazolin-2-iminato- and Imidazolidin-2-iminato Ligands, and their Use as Catalyst Precursors for Ethylene (Co)polymerization

Kotohiro Nomura,* Bijal Kottukkal Bahuleyan, Shu Zhang, Prabhuodeyara M. Veeresha Sharma, Shohei Katao, Atsushi Igarashi, Akiko Inagaki, and Matthias Tamm*

Syntheses, structural analyses of various (imido)vanadium(V) complexes containing 1,3-imidazolin-2-iminato or 1,3-imidazolidin-2-iminato ligands of the type, $V(NR')Cl_2(L)$, have been explored. These complexes showed high activity for ethylene polymerization in the presence of Et_2AlCl: a good correlation between the activity and the ^{51}V NMR chemical shift was observed for the arylimido precatalysts. These complexes exhibited high activity for ethylene/norbornene copolymerization, affording ultrahigh molecular weight copolymers: the copolymerization with 5-ethylidene-2-norbornene proceeded with high activity, efficient comonomer incorporation.

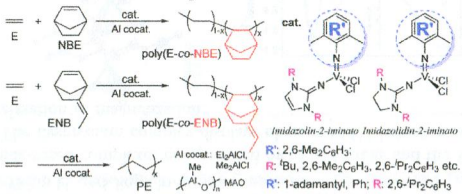

624 S dx.doi.org/10.1021/ic4024585

Rhodium Amidinate Dimers as Structural and Functional Hubs for Multimetallic Assemblies

Daniel Chartrand and Garry S. Hanan*

One to four *fac*-$[Re(bpy)(CO)_3]^+$ chromophores were grafted to a dirhodium tetra-*N*,*N*′-diphenylisonicotinamidinate dimer through its 4-pyridyl moieties. Spectral and electrochemical changes were observed to the dimer base properties. Extended calculations were performed to model these spectral changes, including a solvatochromism effect with acetonitrile. The chromophore emission was reductively quenched by electron transfer from the dirhodium core to the Re(bpy) MLCT state.

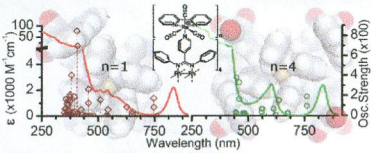

637 Ⓢ dx.doi.org/10.1021/ic402775s

Mo_2 Paddlewheel Complexes Functionalized with a Single MLCT, S_1 Infrared-Active Carboxylate Reporter Ligand: Preparation and Studies of Ground and Photoexcited States

Samantha E. Brown-Xu, Malcolm H. Chisholm,* Christopher B. Durr, Sharlene A. Lewis, Thomas F. Spilker, and Philip J. Young

The compounds Mo_2(*N,N'*-di(*p*-anisyl)formamidinate)$_3$L (L = $O_2CC{\equiv}CPh$, $O_2CC_4H_2SC{\equiv}CH$, and $O_2CC_6H_4$-*p*-CN) have been prepared and characterized. The nature of the excited states has been probed by time-resolved transient absorption and infrared spectroscopies. The observed shifts of $\nu(C{\equiv}X)$ indicate that the negative charge is localized on the single L in the S_1 states, while the T_1 states are $^3Mo_2$ $\delta\delta^*$. Comparisons are made to earlier studies that evaluated the charge distribution in the photoexcited states of *trans*-Mo_2-2,4,6-triisopropylbenzoate-L_2 compounds.

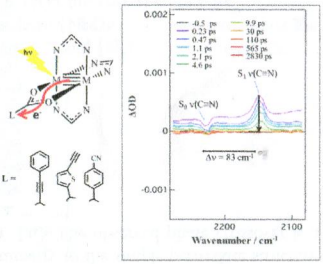

645 Ⓢ dx.doi.org/10.1021/ic402831f

Mechanistic Insights into the C–H Bond Activation of Hydrocarbons by Chromium(IV) Oxo and Chromium(III) Superoxo Complexes

Kyung-Bin Cho, Hyeona Kang, Jaeyoung Woo, Young Jun Park, Mi Sook Seo, Jaeheung Cho,* and Wonwoo Nam*

The C–H bond activation of hydrocarbons by nonheme chromium(IV) oxo and chromium(III) superhydroxo complexes, $[Cr^{IV}(O)(TMC)(Cl)]^+$ and $[Cr^{III}(O_2)(TMC)(Cl)]^+$, has been investigated experimentally and theoretically. The C–H bond activation by the chromium(IV) oxo complex does not occur via the conventional H-atom-abstraction/oxygen-rebound mechanism. The reactivity of the chromium(IV) oxo complex is slightly greater than that of the chromium(III) superoxo complex in the C–H bond activation reactions.

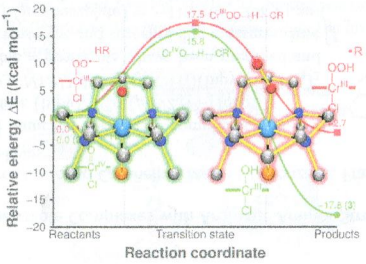

653 Ⓢ dx.doi.org/10.1021/ic402858u

Two-Dimensional Bicapped Supramolecular Hybrid Semiconductor Material Constructed from the Insulators α-Keggin Polyoxomolybdate and 4,4′-Bipyridine

Abishek K. Iyer and Sebastian C. Peter*

The novel organic–inorganic semiconductor hybrid $[SiMo_{14}O_{44}](H4,4'\text{-bpy})_2{\cdot}xH_2O$ having mixed valent Mo atoms and unusual capped α-Keggin structure synthesized by hydrothermal method.

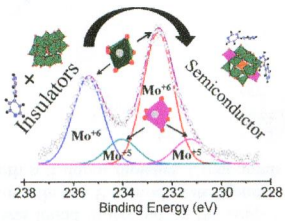

Ⓢ Supporting Information available via online article